Colloid and Polymer Science (2022) 300:509–519
https://doi.org/10.1007/s00396-022-04961-7

ORIGINAL CONTRIBUTION

Facile fabrication of high-performance PA66/MWNT nanocomposite fibers

Xue-Feng Gao[1,2,3] · Wen-Guang Yu[1,2,3] · Na Han[1,2,3] · Xing-Xiang Zhang[1,2,3]

Received: 30 December 2021 / Revised: 21 February 2022 / Accepted: 22 February 2022 / Published online: 7 March 2022

Abstract

Carbon nanotubes (CNTs) are promising polymer-strengthening materials; however, it is difficult to achieve the even distribution of CNTs in polymer matrixes and strong interfacial interactions between CNTs and polymeric chains. In the present work, multi-walled carbon nanotubes (MWNTs), carboxylic multi-walled carbon nanotubes (MWNTs-COOH), amino multi-walled carbon nanotubes (MWNTs-NH_2), and hydroxylated multi-walled carbon nanotubes (MWNTs-OH) were added as reinforcements to the polyamide 66 (PA66) matrix. CNTs were dispersed in the PA66 matrix by a twin-rotor high-speed mixing extruder at 800 rpm. Chips were melted spun and two-step stretched to fabricate nanocomposite fibers. The microstructure and properties of nanocomposite fibers were investigated. It was found that MWNTs-COOH were well dispersed in the PA66 matrix. PA66/MWNTs-COOH nanocomposite fibers exhibited the best mechanical properties. The tensile strength and Young's modulus of PA66/0.3 wt% MWNTs-COOH nanocomposite fibers were ~ 907 MPa and ~ 5.92 GPa, respectively, which were 22.2% and 4.8% higher than those of pure PA66 fibers, respectively.

Keywords Polyamide 66 · Multi-walled carbon nanotubes · Twin-rotor high-speed mixing · Nanocomposite fibers

Introduction

Poly (hexamethylene adipamide) (PA66) has high mechanical strength, good fatigue resistance, and excellent friction resistance. PA66 is widely used in electrical and electronic insulating parts, clothing, automobile tire cords, and packaging products due to its excellent comprehensive performance and good machinability [1, 2]; however, it has a strong water absorption capacity, low modulus, and low impact strength. Therefore, carbon-based nanomaterials are used to enhance the mechanical properties of PA66 fibers [3–8].

Carbon nanotubes (CNTs), which have excellent mechanical, thermal, and electrical properties, are used as superior strength additives [7–10] to enhance the mechanical properties of polymer fibers [11, 12]. It has been reported that the modification of PA66 by CNTs is an effective method to improve the mechanical properties of PA66 fibers [13, 14]. Melt blending [2, 15–18], solution blending [19], and in situ polymerization [13, 14, 20] are generally used to fabricate CNTs-reinforced polymer nanocomposites. Mai et al. [15] fabricated PA66/MWNT nanocomposite fibers by melt spinning. In comparison to pure PA66 fibers, the tensile fracture strength and Young's modulus of PA66/1 wt% MWNT composite fibers increased by 40% and 66%, respectively. Chen et al. [16] fabricated PA66/MWNT composite fibers by ball milling and melt spinning and investigated the effects of unmodified (U-MWNTs), acid-modified (MWNTs-COOH), and sodium dodecylbenzene sulfonate-modified (MWNTs-SDBS) MWNTs on the mechanical and thermal properties of PA66. The tensile strengths of PA66/0.1 wt% MWNTs-SDBS and PA66/0.1 wt% MWNTs-COOH composite fibers were 27% and 24% higher than those of PA66 fibers, respectively. Zhang et al. [13] aminated MWNTs by the Diels–Alder (D-A) reaction and fabricated MWNTs-NH_2/PA66 composite fibers by in situ polymerization. The as-prepared MWNTs-NH_2 fibers were evenly dispersed in the PA66 matrix and had a strong interfacial interaction with

✉ Na Han
hanna@tjpu.edu.cn

✉ Xing-Xiang Zhang
zhangpolyu@aliyun.com

1 School of Material Science and Engineering, Tiangong University, Tianjin 300387, China

2 Tianjin Municipal Key Laboratory of Advanced Fiber and Energy Storage, Tianjin, China

3 Advanced Textile and Composite Key Lab of the Ministry of Education, Tianjin, China

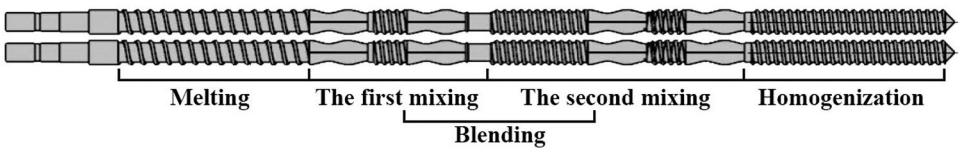

Fig. 1 Screw structure of the twin-rotor extruder

polymer chains. The tensile strength of PA66/0.5 wt% MWNTs-NH_2 composite fibers (~ 611 MPa) was 140% higher than that of pure PA66 fibers. Zhang et al. [14] fabricated PA66/3-aminopropyl terminated polydimethylsiloxane (PA66/APDMS)-carboxylic multi-walled carbon nanotube (CMWNT) nanocomposites by in situ polymerization and obtained PA66/APDMS-CMWNT composite fibers by melt spinning. The tensile fracture strength and Young's modulus of the fabricated composite fibers were 559 MPa and 9.5 GPa, respectively, which were 167% and 631% higher than those of pure PA66 fibers, respectively.

However, due to the incompatibility between CNTs and polymer chains [6–8], the presence of powerful van der Waals forces between CNTs, and the large specific surface area and aspect ratio of CNTs, CNTs easily agglomerate in polymer matrixes. Among different methods, in situ polymerization can effectively improve the dispersion of CNTs in polymer matrixes and improve the mechanical properties of nanocomposites. It has been demonstrated that with the increase of the loading of MWNTs, the molecular weight of attached polymer chains decreases [21]. This happens because the surface of MWNTs contains some active functional groups, which react with polymer monomers and prevent polymerization. In addition, MWNT nanoparticles reduce the probability of collision between polymer monomers and decrease the final molecular weight [22]. The dispersion effect of CNTs in common melt-blending is poor, resulting in poor nanocomposite properties [7, 15, 17, 18]. Therefore, it is necessary to employ a simple and effective method to achieve the uniform dispersion of CNTs in polymer matrixes and maintain the inherent properties of CNTs. Twin-rotor high-speed mixing extruders are high polymerization mixing equipment [23]. In comparison to traditional mixing equipment, twin-rotor high-speed mixing extruders have a two-part intersection zone in the rotor element, facilitating the complete blending between reinforcements and polymer matrixes. The screw speed can reach 1000 rpm.

In the present work, a twin-rotor high-speed mixing extruder (ET30) was used to effectively disperse MWNTs in the PA66 matrix. The effects of the twin-rotor speed and the type and loading of MWNTs on the mechanical properties of PA66/MWNT nanocomposite fibers were investigated. PA66/MWNT nanocomposite fibers with excellent mechanical properties were successfully fabricated. This work provides a new method for the industrial fabrication of high-performance nanocomposite fibers.

Experimental section

Materials

PA66 (EPR27; melt index = 10.8 g/10 min, relative viscosity = 2.67) was supplied by Pingdingshan Shenma Co. Ltd., China. MWNTs, MWNTs-COOH (3.86 wt% carboxylation of carbon atoms), MWNTs-NH_2 (0.45 wt% carbon atom amination), and MWNTs-OH (5.58 wt% hydroxylated carbon atoms) with > 95% purity were procured from Beijing Deke Daojin Science and Technology Co. Ltd., China.

Fabrication of PA66/CNT nanocomposite chips

Vacuum-dried PA66 chips were mixed with CNTs (MWNTs, MWNTs-COOH, MWNTs-NH_2, and MWNTs-OH) by a twin-rotor high-speed mixing extruder (Fig. 1), and PA66/CNT nanocomposite chips were fabricated at 200 rpm and 800 rpm. The temperature parameters of the twin-rotor high-speed mixing extruder are presented in Table 1. The loadings of CNTs were 0.1 wt%, 0.2 wt%, 0.3 wt%, 0.4 wt%, and 0.5 wt%. The as-prepared PA66/CNT nanocomposite chips were dried in a vacuum oven at 130 °C for 24 h to decrease the moisture content to less than 50 ppm for spinning.

Fabrication of PA66/CNT nanocomposite fibers

The spinning temperature was set at 290 °C, the diameter of the spinneret (24 holes) was 0.3 mm, and the winding rate was 350 m/min. In order to further improve the orientation and crystallinity of nanocomposite fibers, a two-step drawing process was adopted. In the high-speed drawing stage, the as-spun fibers were drawn five times by four guidewire rollers (parameters: GR1: 85 °C, 70 m/min; GR2: 170 °C, 280 m/min; GR3: 210 °C, 350 m/min; GR4: 80 °C, 350 m/min). In the low-speed drawing stage, the as-obtained fibers were stretched to 1.2 times their original length by three sets of guidewire

Table 1 Granulation temperatures of the twin-rotor high-speed mixing extruder

Sub-region	Region 1	Region 2	Region 3	Region 4	Region 5	Region 6
Temperature (°C)	270	270	280	280	280	290

rollers (GR5: 70 °C, 20 m/min; GR6: 150 °C, 23 m/min; GR7: 200 °C, 24 m/min). The total drawing ratio of the first guide roller (GR1) and the last guide roller (GR7) was 1:6.

Characterization

X-ray diffraction (XRD) was carried out by a Rigaku D/MAX-GA diffractometer (Japan) under filtered Cu-Kα radiation ($\lambda = 0.15406$ nm). Raman spectra were registered by a Raman microscope equipped with a laser source of 532-nm wavelength (Horiba, XploRA PLUS, Japan). Fourier-transformed infrared (FTIR) spectra were detected at 400–4000 cm^{-1} by a Bruker TERSOR37 spectrometer (Germany). The thermal properties of nanocomposite fibers were characterized by a differential scanning calorimeter (DSC; Netzsch 204 F1, Germany). Field-emission scanning electron microscopy (SEM; ZEISS Gemini SEM500, Germany) and transmission electron microscopy (TEM; Hitachi H-7650, Japan) were employed to reveal the microstructures of nanocomposite fibers at an acceleration voltage of 100 kV. The mechanical properties of nanocomposite fibers were tested by an electronic tensile strength testing machine (Laizhou, LLY-088, China). The fiber length was 10 mm, the stretching rate was 10 mm/min, and the average number of tests was 10.

Results and discussion

Morphology of different carbon nanotubes

Figure 2 displays the TEM images of MWNTs, MWNTs-COOH, MWNTs-NH_2, and MWNTs-OH. The external diameters and lengths of different CNTs ranged between 20–40 nm and 1–5 μm, respectively, and their aspect ratio was less than 250. The entanglement and stacking of CNTs were significantly reduced by the twin-rotor extruder, conducing the dispersion of CNTs in the PA66 matrix.

Figure 3 presents the FTIR spectra of MWNTs, MWNTs-COOH, MWNTs-NH_2, and MWNTs-OH. The peaks at 1551 cm^{-1} and 1202 cm^{-1} appeared from the stretching vibration

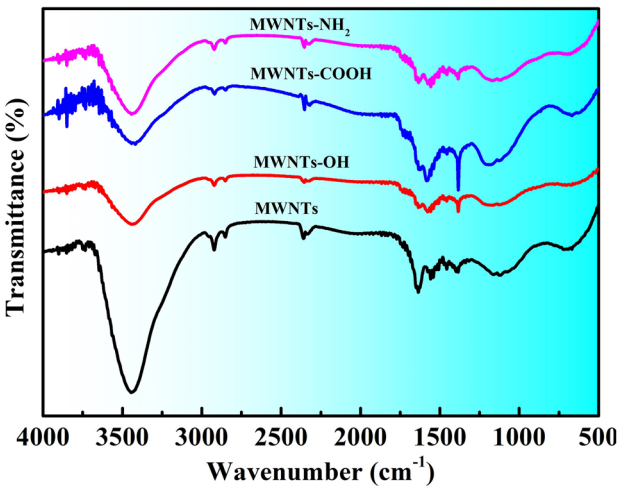

Fig. 3 FTIR spectra of MWNTs, MWNTs-COOH, MWNTs-NH_2, and MWNTs-OH

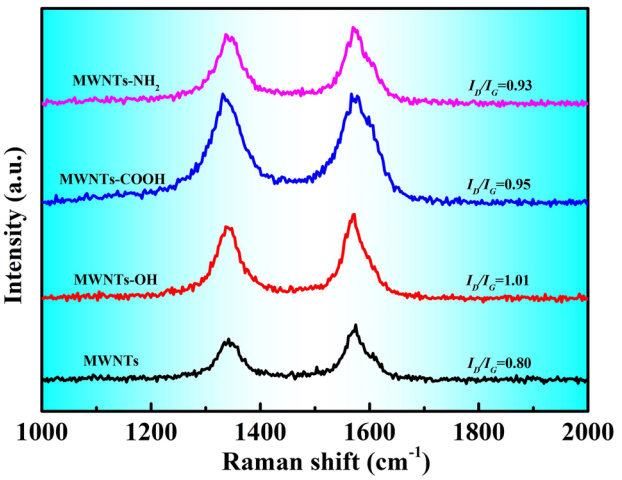

Fig. 4 Raman spectra of MWNTs, MWNTs-COOH, MWNTs-NH_2, and MWNTs-OH

of -C=C- on the carbon skeleton. The C=O and C-O stretching vibration peaks of MWNTs-COOH (characteristic peaks of

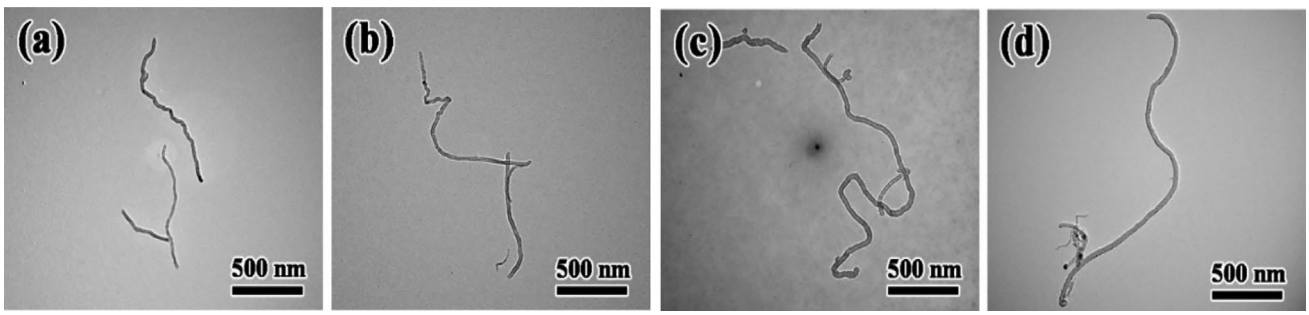

Fig. 2 TEM images of (**a**) MWNTs, (**b**) MWNTs-COOH, (**c**) MWNTs-NH_2, and (**d**) MWNTs-OH

-COOH) appeared at 1727 cm^{-1} and 1130 cm^{-1}, respectively. In MWNTs-OH, the characteristic peak of -OH, the bending vibration peak of -OH, and the stretching vibration peak of C-O were detected at 3440 cm^{-1}, 1170 cm^{-1}, and 1400 cm^{-1}, respectively. In MWNTs-NH_2, the stretching vibration peaks of C-N and -CH_2 appeared at 1157 cm^{-1} and 2923 cm^{-1}, respectively [24, 25].

The Raman spectra of MWNTs, MWNTs-COOH, MWNTs-NH_2, and MWNTs-OH are shown in Fig. 4. The G and D peaks were detected at 1580 cm^{-1} and 1350 cm^{-1}, respectively. The G peak is related to the in-plane stretching vibration of sp^2-hybridized carbon atoms, and the D peak is related to lattice defects in carbon atoms [26]. Generally, the I_D/I_G ratio is used

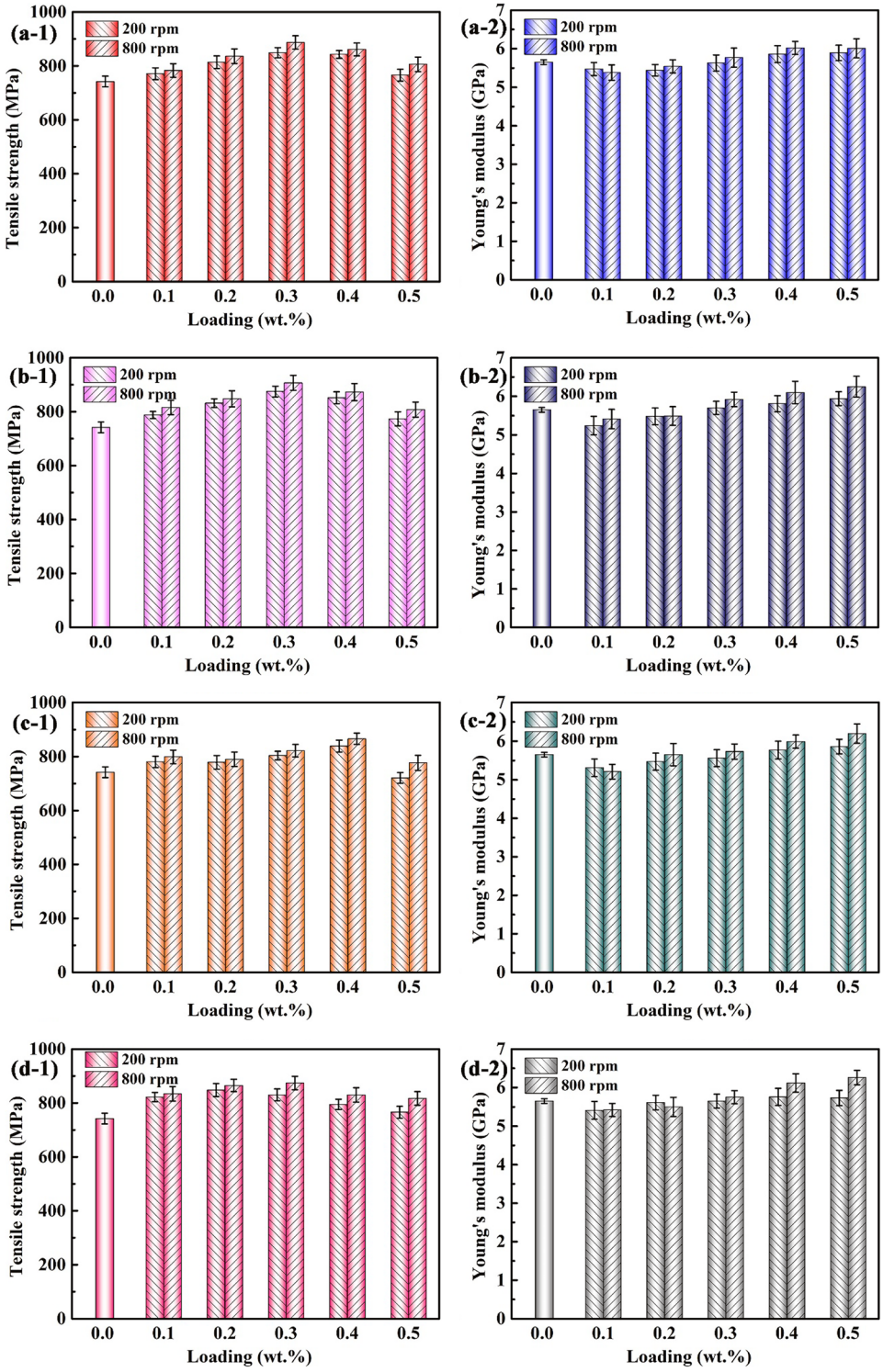

Fig. 5 Mechanical properties of pure PA66 and nanocomposite fibers: (**a**) PA66/MWNTs, (**b**) PA66/MWNTs-COOH, (**c**) PA66/MWNTs-OH, and (**d**) PA66/MWNTs-NH_2

to describe defects in carbon materials [27, 28]. The I_D/I_G value of functionalized CNTs was larger than that of pure ones, indicating that more sp^3-hybridized carbon atoms existed on the surface of functionalized CNTs. When functionalized CNTs were added to the PA66 matrix as reinforcement elements, the agglomeration and entanglement of CNTs in the polymer matrix were greatly reduced.

Mechanical properties of nanocomposite fibers

Figure 5 and Table 2 present the mechanical properties of pure PA66 fibers and nanocomposite fibers fabricated by adding different mass fractions of MWNTs, MWNTs-COOH, MWNTs-OH, and MWNTs-NH_2. The mechanical strength of the nanocomposite fibers blended at 800 rpm was superior to that of the nanocomposite fibers blended at 200 rpm. This happened because CNTs were more evenly dispersed in the PA66 matrix at 800 rpm. Furthermore, when the loading of MWNTs-COOH was 0.3 wt%, the nanocomposite fibers showed the best mechanical properties.

It is noticeable from Fig. 5 that when the loading of MWNTs was lower than 0.3 wt%, the tensile fracture strength of nanocomposite fibers increased with the increase of MWNT loading. However, as the loading of MWNTs continued to increase, the tensile fracture strength decreased. It happened mainly due to the winding of MWNTs, making their dispersion in the polymer matrix worse and causing stress concentration under external stress [29, 30]. When the loading of MWNTs-COOH was 0.3 wt%, the tensile fracture strength and Young's modulus of nanocomposite fibers were 907 MPa and 5.92 GPa, respectively, which were 22.2% and 4.8% higher than those of pure PA66 fibers, respectively. This happened because under the action of high rotational speed, -COOH- bonds of MWNTs-COOH were chemically bonded with PA66 chains through heating and shearing and formed amide bonds; thus, MWNTs-COOH had a better interfacial interaction with the PA66 matrix, enhancing the strength of nanocomposite fiber. The elongation at break of the nanocomposite fibers prepared at the 800-rpm rotating speed is greater than that at 200-rpm rotating speed. This is because at 800 rpm, the CNTs can be more uniformly dispersed in the PA66 matrix, and has a good interface with the PA66 matrix, so that the load can be effectively transferred to the CNTs, and it is not easy to generate stress concentration when it is subjected to external force, which makes the elongation at break larger.

When the loading of CNTs was 0.3 wt%, the tensile fracture strength reached a maximum. It has been reported that when the loading of CNTs reaches 0.5 wt% during wet spinning and melt spinning, nanocomposite fibers yield the maximum tensile fracture strength [12]. Therefore, it could be speculated that the twin-rotor high-speed mixer with its ultra-high speed (over 600 rpm) evenly dispersed CNTs in the PA66 matrix,

Table 2 Mechanical properties of pure PA66 and nanocomposite fibers

Specimen	Tensile strength (MPa)		Young's modulus (GPa)		Elongation (%)	
	200 rpm	800 rpm	200 rpm	800 rpm	200 rpm	800 rpm
PA66	742 ± 20		5.65 ± 0.06		13 ± 1	
PA66/0.1 wt% MWNTs	771 ± 22	783 ± 25	5.47 ± 0.17	5.38 ± 0.20	12 ± 2	14 ± 2
PA66/0.2 wt% MWNTs	814 ± 23	836 ± 27	5.44 ± 0.15	5.54 ± 0.17	12 ± 2	11 ± 1
PA66/0.3 wt% MWNTs	849 ± 19	887 ± 25	5.63 ± 0.21	5.77 ± 0.25	14 ± 1	13 ± 2
PA66/0.4 wt% MWNTs	843 ± 14	861 ± 24	5.86 ± 0.22	6.02 ± 0.17	11 ± 2	16 ± 3
PA66/0.5 wt% MWNTs	766 ± 22	806 ± 27	5.89 ± 0.20	6.01 ± 0.25	12 ± 3	15 ± 2
PA66/0.1 wt% MWNTs-COOH	788 ± 13	816 ± 27	5.24 ± 0.24	5.41 ± 0.25	13 ± 3	15 ± 2
PA66/0.2 wt% MWNTs-COOH	832 ± 16	848 ± 30	5.48 ± 0.22	5.49 ± 0.24	15 ± 2	14 ± 1
PA66/0.3 wt% MWNTs-COOH	875 ± 20	907 ± 28	5.70 ± 0.17	5.92 ± 0.19	14 ± 3	17 ± 2
PA66/0.4 wt% MWNTs-COOH	852 ± 22	873 ± 32	5.81 ± 0.21	6.10 ± 0.29	14 ± 2	16 ± 1
PA66/0.5 wt% MWNTs-COOH	774 ± 26	808 ± 28	5.94 ± 0.18	6.25 ± 0.27	13 ± 1	17 ± 2
PA66/0.1 wt% MWNTs-OH	781 ± 21	799 ± 25	5.31 ± 0.23	5.21 ± 0.19	12 ± 1	12 ± 2
PA66/0.2 wt% MWNTs-OH	779 ± 25	790 ± 27	5.47 ± 0.22	5.65 ± 0.29	15 ± 1	19 ± 3
PA66/0.3 wt% MWNTs-OH	804 ± 16	822 ± 23	5.56 ± 0.22	5.73 ± 0.20	14 ± 2	16 ± 2
PA66/0.4 wt% MWNTs-OH	839 ± 22	866 ± 21	5.77 ± 0.23	5.99 ± 0.17	13 ± 1	17 ± 2
PA66/0.5 wt% MWNTs-OH	721 ± 20	777 ± 28	5.86 ± 0.19	6.20 ± 0.25	13 ± 3	15 ± 1
PA66/0.1 wt% MWNTs-NH_2	822 ± 17	834 ± 27	5.41 ± 0.23	5.42 ± 0.17	15 ± 2	13 ± 2
PA66/0.2 wt% MWNTs-NH_2	848 ± 24	865 ± 23	5.61 ± 0.19	5.50 ± 0.25	12 ± 2	12 ± 2
PA66/0.3 wt% MWNTs-NH_2	830 ± 22	874 ± 25	5.65 ± 0.18	5.75 ± 0.17	14 ± 1	15 ± 2
PA66/0.4 wt% MWNTs-NH_2	795 ± 19	830 ± 27	5.76 ± 0.22	6.12 ± 0.24	15 ± 2	13 ± 1
PA66/0.5 wt% MWNTs-NH_2	766 ± 22	817 ± 25	5.73 ± 0.20	6.26 ± 0.19	13 ± 1	14 ± 2

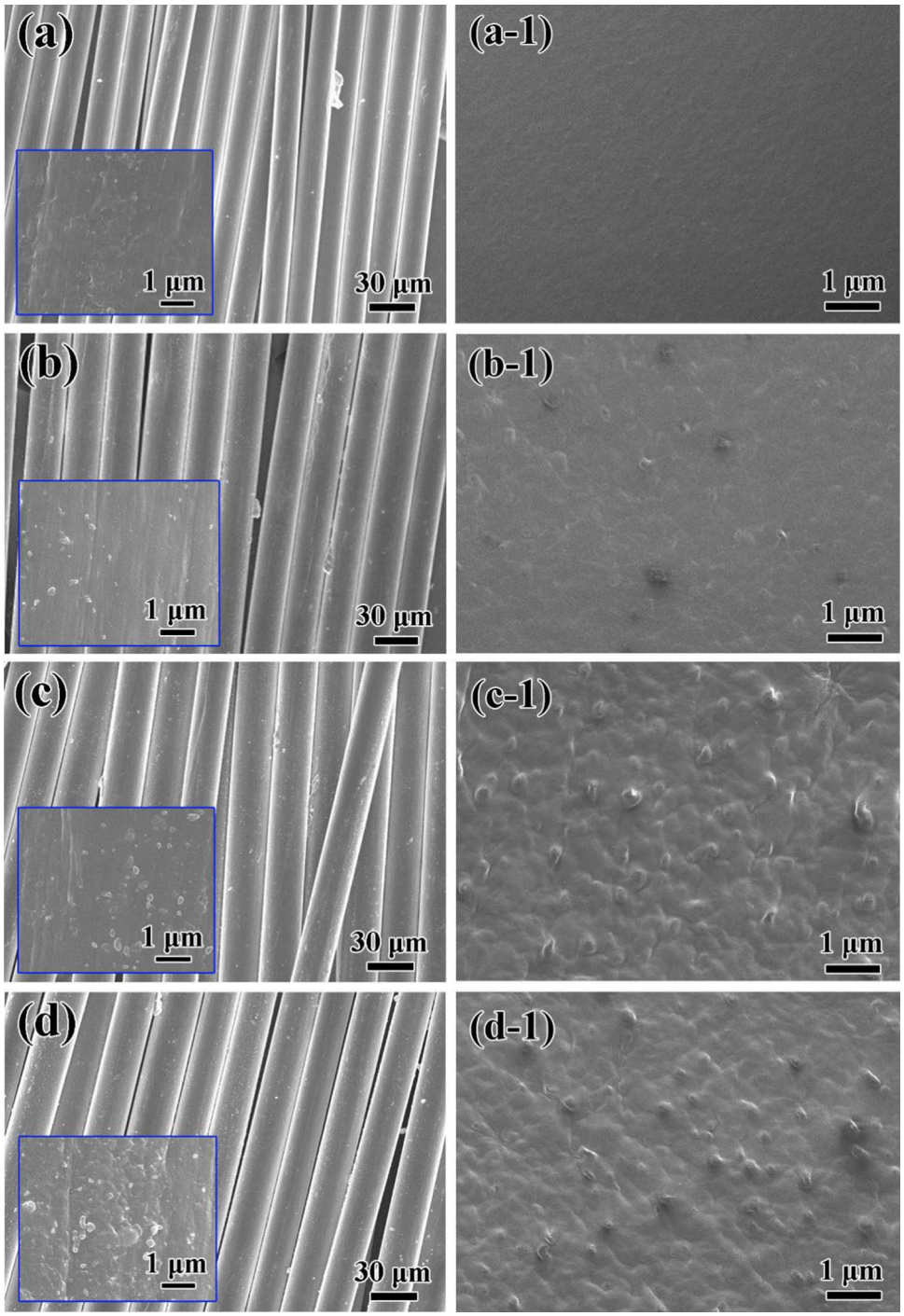

Fig. 6 SEM images of the surface and fracture surface of nanocomposite fibers: (**a**, a-1) PA66, (**b**, b-1) 0.1 wt% MWNTs-COOH, (**c**, c-1) 0.3 wt% MWNTs-COOH, (**d**, d-1) 0.5 wt% MWNTs-COOH

reduced the loading amount of CNTs, improved the utilization rate, and greatly enhanced the mechanical properties of nanocomposite fibers.

Dispersion of MWNTs-COOH in PA66 nanocomposite fibers

The mechanical properties of PA66/CNT nanocomposite fibers were mainly related to the dispersion and compatibility of CNTs in the PA66 matrix. The more even the dispersion of CNTs in the polymer matrix, the better the compatibility and the higher the mechanical properties of nanocomposite fibers. According to the obtained mechanical properties (Table 2), PA66/MWNTs-COOH nanocomposite fibers with the best mechanical properties were used for further analysis. Figure 6 displays the SEM images of pure PA66 fibers and PA66/MWNTs-COOH nanocomposite fibers with MWNTs-COOH loadings of 0.1 wt%, 0.3 wt%, and

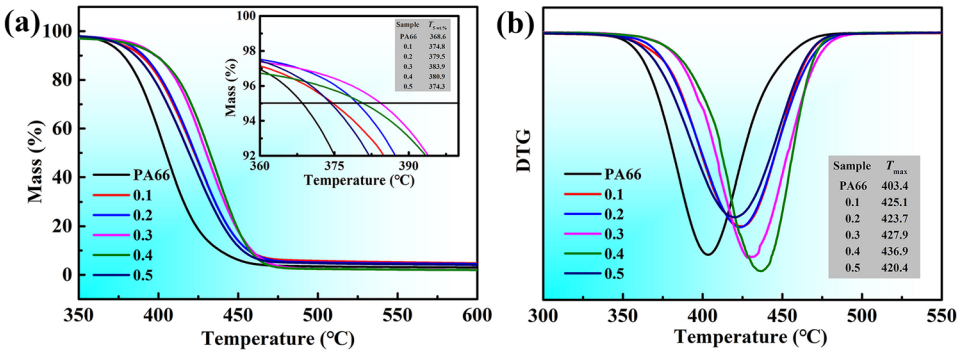

Fig. 7 TGA and DTG curves of pure PA66 and PA66/MWNTs-COOH nanocomposite fibers

0.5 wt% (white points indicate dispersed MWNTs-COOH in the PA66 matrix) [24]. When the loading was 0.3 wt%, MWNTs-COOH dispersed evenly in the PA66 matrix without agglomeration. When nanocomposite fibers were subjected to external stress, MWNTs-COOH effectively transferred the stress, improving the tensile fracture strength of fibers. When the loading was 0.5 wt%, MWNTs-COOH agglomerated in the PA66 matrix, and stress concentration easily occurred under external stress, leading to a decline of mechanical properties.

Thermal and crystallization properties of nanocomposite fibers

Figure 7 shows the TG and DTG curves of pure PA66 and PA66/MWNTs-COOH nanocomposite fibers, and the corresponding data are listed in Table 3. The decomposition trends of pure PA66 and PA66/MWNTs-COOH nanocomposite fibers were similar. The initial decomposition temperature was set when there was 5 wt% ($T_{5\ wt\%}$) fiber weight loss. When the loading of MWNTs-COOH was below 0.3 wt%, the $T_{5\ wt\%}$ temperature of nanocomposite fibers increased with the increase of MWNTs-COOH loading. At 0.3 wt%, the $T_{5\ wt\%}$ value reached 383.9 °C because MWNTs-COOH were most evenly dispersed in the matrix at this dosage, MWNTs-COOH had strong adsorption during thermal decomposition, and the hydrogen bonding between MWNTs-COOH and the PA66 matrix was the strongest.

Table 3 TG data of pure PA66 and PA66/MWNTs-COOH nanocomposite fibers

Specimen	$T_{5wt\%}$ (°C)	T_{max} (°C)
PA66	368.6	403.4
PA66/0.1 wt% MWNTs-COOH	374.7	425.1
PA66/0.2 wt% MWNTs-COOH	379.5	423.7
PA66/0.3 wt% MWNTs-COOH	383.9	427.9
PA66/0.4 wt% MWNTs-COOH	380.9	436.9
PA66/0.5 wt% MWNTs-COOH	374.3	420.4

When the loading of MWNTs-COOH continued to increase to 0.5 wt%, $T_{5\ wt\%}$ of nanocomposite fibers decreased. Because MWNTs-COOH agglomerated, the dispersion and compatibility of MWNTs-COOH in the PA66 matrix became worse, and the adsorption effect during decomposition deteriorated. The $T_{5\ wt\%}$ of nanocomposite fibers first increased and then decreased. The temperature of the maximum weight loss rate (T_{max}) of nanocomposite fibers also first increased and then decreased, and the value reached 427.9 °C at 0.3 wt%, which was 24.5 °C higher than that of pure PA66 fibers.

Figure 8 presents the DSC heating and cooling curves of pure PA66 and PA66/MWNTs-COOH nanocomposite fibers. The tensile fracture strength of the fibers was positively correlated with their crystallinity. The crystallinity of the fibers was calculated using Eq. (1), and the obtained data are listed in Table 4. Little difference was noticed between the melting temperatures (T_m) of pure PA66 and PA66/MWNTs-COOH nanocomposite fibers, implying that the loading of MWNTs-COOH had little effect on the lamellar thickness and spherulite size of nanocomposite fibers [31]. However, PA66/MWNTs-COOH nanocomposite fibers had a higher crystallization temperature than pure PA66 fibers. MWNTs-COOH could be used as a heterogeneous nucleating agent to provide more crystallization nucleation sites, accelerate the crystallization rate, improve the crystallinity, and enhance the mechanical strength of nanocomposite fibers. The two-step drafting method improves the drawing process, prolongs the annealing time of the fiber, increases the α-type crystal structure in the composite fiber, improves the crystallinity of the composite fiber, at the same time improves the orientation of the crystalline region and the amorphous region, and achieves a significant improvement in the mechanical properties of composite fibers [32, 33].

$$X_c = \frac{\Delta H_m}{\Delta H_m^0 (1 - \alpha\%)} \quad (1)$$

where X_c is crystallinity, ΔH_m is the melting enthalpy, ΔH_m^0 is the theoretical melting enthalpy of the complete crystallization

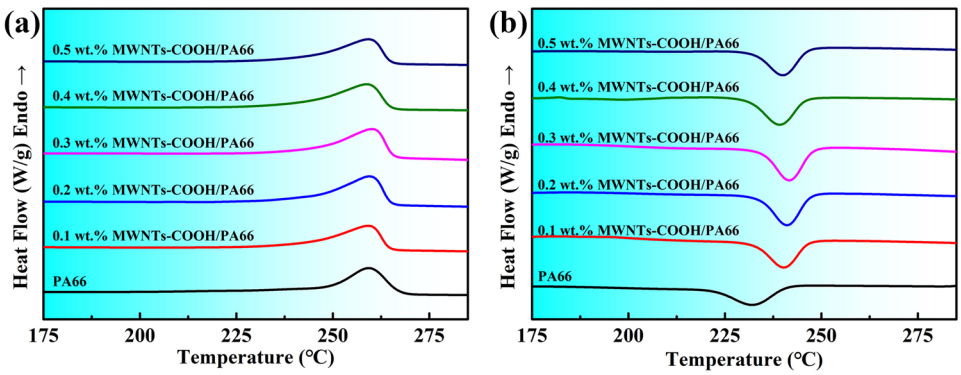

Fig. 8 DSC curves of the (**a**) melting and (**b**) cooling behavior of PA66 and PA66/MWNTs-COOH nanocomposite fibers

of PA66 (194.69 J/g), and α is the loading content of MWCNTs in nanocomposite fibers.

When the loading of MWNTs-COOH was 0.3 wt%, PA66/MWNTs-COOH nanocomposite fibers had the maximum crystallinity of 40.3% and also the maximum mechanical strength. As the content of MWNTs-COOH further increased, the mechanical strength of nanocomposite fibers decreased because of the agglomeration of MWNTs-COOH in the matrix, hindering the movement of PA66 molecular chains, decreasing the number of crystallization sites, impeding the crystal growth, and reducing the crystallinity [20]. The crystallinity of nanocomposite fibers was positively correlated with their mechanical strength, and the maximum crystallinity corresponded to the optimal mechanical properties of nanocomposite fibers.

PA66 is a polycrystalline polymer with two crystal forms—α- and β-crystal planes [15]. Figure 9 presents the XRD curves of pure PA66 and PA66/MWNTs-COOH nanocomposite fibers. The diffraction peaks near $2\theta = 20.3°$ and 23.4° appeared from the (100) α-crystal plane (including β-crystals) and the (010)(110) crystal plane, respectively. The peak height ratio of the (100) and (010)(110) planes was used to determine the crystal type. With the increase of the loading of MWNTs-COOH, the peak height ratio of the (100) and (010)(110) planes of nanocomposite fibers first decreased and then increased. This happened because a small amount of MWNTs-COOH fibers was uniformly dispersed in the PA66 matrix and served as crystallization sites for heterogeneous nucleation; thus, crystals grew along the (010)(110) plane. The grain sizes of pure PA66 and PA66/MWNTs-COOH nanocomposite fibers were calculated using the Scherrer formula, and the corresponding data are presented in Table 5. In comparison to pure PA66 fibers, the grain size of nanocomposite fibers decreased along the (100) plane and increased along the (010)(110) plane, indicating that the addition of MWNTs-COOH to the PA66 matrix had a heterogeneous nucleation effect and promoted the crystal growth along the (010)(110) plane; thus, the degree of crystallization became more perfect. The oriented lamellar structure of the PA66 matrix nucleated on the surface of MWNTs in the form of transcrystalline interphases. However, when the amount of MWNTs exceeded 0.3 wt%, the number of nucleation sites increased, and one-dimensional transcrystalline interphases intersected each other, destroying the regular crystal structure, impeding

Table 4 DSC data of pure PA66 and PA66/MWNTs-COOH nanocomposite fibers

Specimen	T_m (°C)	ΔH_m (J/g)	T_c (°C)	X_c (%)
PA66	259.6	64.28	232.0	33.0
PA66/0.1 wt% MWNTs-COOH	259.2	69.24	240.2	35.6
PA66/0.2 wt% MWNTs-COOH	259.5	77.68	241.1	39.9
PA66/0.3 wt% MWNTs-COOH	260.2	78.44	241.7	40.3
PA66/0.4 wt% MWNTs-COOH	258.8	71.49	239.2	36.7
PA66/0.5 wt% MWNTs-COOH	259.3	67.95	240.0	34.9

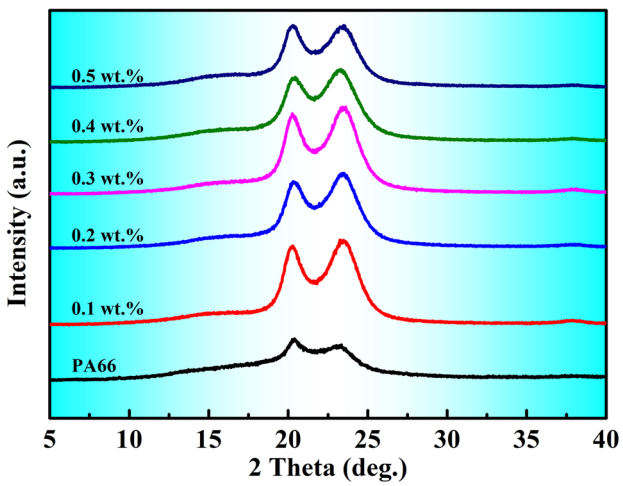

Fig. 9 XRD patterns of pure PA66 and PA66/MWNTs-COOH nanocomposite fibers

Table 5 XRD data of pure PA66 and PA66/MWNTs-COOH nanocomposite fibers

Specimen	2θ (°)		FWHM		D100 (nm)	D010 (nm)
	α1	α2	α1	α2		
PA66	20.40	23.40	0.666	0.997	11.99	8.05
PA66/0.1 wt% MWNTs-COOH	20.26	23.44	0.887	1.035	9.00	7.75
PA66/0.2 wt% MWNTs-COOH	20.54	23.68	0.867	0.934	9.21	8.59
PA66/0.3 wt% MWNTs-COOH	19.98	23.28	0.975	0.914	10.0	8.78
PA66/0.4 wt% MWNTs-COOH	20.38	23.32	0.918	0.968	8.09	8.29
PA66/0.5 wt% MWNTs-COOH	20.30	23.50	0.889	1.025	8.98	7.83

the growth of complete crystals [34], leading to poor crystallization, and deteriorating the mechanical properties nanocomposite fibers.

Figure 10 exhibits the DMA curves of pure PA66 and PA66/MWNTs-COOH nanocomposite fibers. The size of the loss factor was positively correlated with the volume of the amorphous region of the fibers [35]. When the loading of MWNTs-COOH was in the range of 0.1–0.5 wt%, the value of tanδ of nanocomposite fibers first decreased and then increased with the increase of the loading content; however, these values were smaller than those of pure PA66 fibers, indicating that the addition of MWNTs-COOH reduced the volume of the amorphous zone and increased the volume of the crystalline zone of nanocomposite fibers. The tanδ (0.078) of PA66/0.3 wt% MWNTs-COOH nanocomposite fibers was the smallest; thus, the free volume of PA66/0.3 wt% MWNTs-COOH nanocomposite fibers was the smallest and the crystal volume was the largest at 0.3 wt%. At 0.5 wt%, the tanδ value reached 0.094, the amorphous region became larger, and the crystalline region became smaller; these findings are consistent with the DSC results. In addition, the peak temperature of the loss factor corresponded to the T_g of nanocomposite fibers. The T_g of pure PA66 fibers

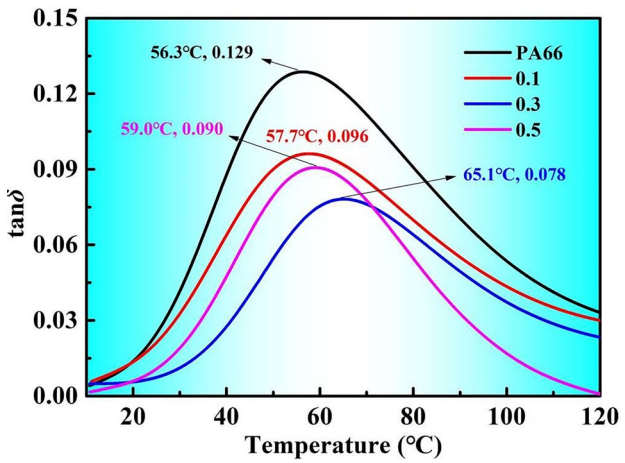

Fig. 10 tanδ versus temperature curves for nanocomposite fibers with different MWNTs-COOH contents

was 56.3 °C. With the addition of MWNTs-COOH, the T_g of nanocomposite fibers first increased and then decreased, and the value reached a maximum of 65.1 °C at the dosage of 0.3 wt%.

Conclusions

CNT (MWNTs, MWNTs-COOH, MWNTs-NH_2, MWNTs-OH)-reinforced PA66 nanocomposite fibers were fabricated by mixing granulation on a twin-rotor high-speed mixing extruder. Melt spinning and two-step drawing were carried out at 200 rpm and 800 rpm. The dispersion of CNTs in the PA66 matrix was significantly improved at 800 rpm, and the mechanical properties of nanocomposite fibers fabricated at 800 rpm were superior. The tensile strength and Young's modulus of PA66/0.3 wt% MWNTs-COOH nanocomposite fibers were 907 MPa and 5.92 GPa, respectively, which were 22.2% and 4.8% higher than those of pure PA66 fibers, respectively. Moreover, the entangled agglomeration of 0.3 wt% MWNTs-COOH nanocomposite fibers was not detected in the PA66 matrix. Among all fibers, the dispersion and compatibility of 0.3 wt% MWNTs-COOH fibers in the PA66 matrix were the best. The $T_{5\ wt\%}$ and T_{max} of 0.3 wt% MWNTs-COOH nanocomposite fibers were 383.9 °C and 427.9 °C, respectively, which were 15.3 °C and 24.5 °C higher than those of pure PA66 fibers, respectively. The crystallinity of PA66/0.3 wt% MWNTs-COOH nanocomposite fibers (40.3%) was 7.3% higher than that of pure PA66 fibers.

Funding This work was supported by the Tianjin Science and Technology Military and Civilian Integration key special project (18ZXJMTG00110).

Declarations

Conflict of interest The authors declare no competing interests.

References

1. Masood MT, Papadopoulou EL, Heredia-Guerrero JA, Bayer IS, Athanassiou A, Ceseracciu L (2017) Graphene and polytetrafluoroethylene synergistically improve the tribological properties

and adhesion of nylon 66 coatings. Carbon 123:26–33. https://doi.org/10.1016/j.carbon.2017.07.026
2. Kim J, Oh J, Lee KY, Jung I, Park M (2017) Dispersion of graphene-based nanocarbon fillers in polyamide 66 by dry processing and its effect on mechanical properties. Compos Part B-Eng 114:445–456. https://doi.org/10.1016/j.compositesb.2017.01.054
3. Bellenger V, Tcharkhtchi A, Castaing P (2006) Thermal and mechanical fatigue of a PA66/glass fibers composite material. Int J Fatigue 28:1348–1352. https://doi.org/10.1016/j.ijfatigue.2006.02.031
4. Chang QX, Zhao HJ, He RQ (2017) The addition of clay on the mechanical properties of surface-treated CF-filled PA66 composites. Surf Interface Anal 49:837–842. https://doi.org/10.1002/sia.6230
5. Xu X, Li B, Lu H, Zhang Z, Wang H (2007) The interface structure of nano-SiO2/PA66 composites and its influence on material's mechanical and thermal properties. Appl Surf Sci 254:1456–1462. https://doi.org/10.1016/j.apsusc.2007.07.014
6. Ajayan PM, Tour JM (2007) Materials science—nanotube composites. Nature 447:1066–1068. https://doi.org/10.1038/4471066a
7. Kinloch IA, Suhr J, Lou J, Young RJ, Ajayan PM (2018) Composites with carbon nanotubes and graphene: an outlook. Science 362:547–553. https://doi.org/10.1126/science.aat7439
8. Coleman JN, Khan U, Blau WJ, Gun'Ko Y (2006) Small but strong: a review of the mechanical properties of carbon nanotube–polymer composites. Carbon 44:1624–1652. https://doi.org/10.1016/j.carbon.2006.02.038
9. Tran TQ, Fan Z, Mikhalchan A, Liu P, Duong HM (2016) Post-treatments for multifunctional property enhancement of carbon nanotube fibers from the floating catalyst method. ACS Appl Mater Interfaces 8:7948–7956. https://doi.org/10.1021/acsami.5b09912
10. Tian C, Yu-Zhou W, Hai-Hui L, Xing-Xiang Z (2017) Melt-spinning of carboxylated MWNTs-reinforced polyamide 6 fibers with solid mixing nanocomposites. Polym Compos 39:4298–4309. https://doi.org/10.1002/pc.24510
11. Qian H, Kalinka G, Chan KLA, Kazarian SG, Greenhalgh ES, Bismarck A, Shaffer MSP (2011) Mapping local microstructure and mechanical performance around carbon nanotube grafted silica fibres: methodologies for hierarchical composites. Nanoscale 3:4759–4767. https://doi.org/10.1039/c1nr10497g
12. Mahmood N, Islam M, Hameed A, Saeed S, Khan AN (2014) Polyamide-6-based composites reinforced with pristine or functionalized multi-walled carbon nanotubes produced using melt extrusion technique. J Compos Mater 48:1197–1207. https://doi.org/10.1177/0021998313484779
13. Zhang J, Gao X, Zhang X, Liu H, Zhang X (2019) Polyamide 66 and amino-functionalized multi-walled carbon nanotube composites and their melt-spun fibers. J Mater Sci 54:1–13. https://doi.org/10.1007/s10853-019-03619-0
14. Zhang J, Yu WG, Zhang XY, Gao XF, Liu HH, Zhang XX (2020) Enhancement of physical and mechanical properties of polyamide 66 fibers using polysiloxane-functionalized multi-walled carbon nanotubes. J Appl Polym Sci 138:50170. https://doi.org/10.1002/app.50170
15. Mai F, Pan DD, Gao X, Yao MJ, Deng H, Wang K, Chen F, Fu Q (2011) Extension-induced mechanical reinforcement in melt-spun fibers of polyamide 66/multiwalled carbon nanotube composites. Polym Int 60:1646–1654. https://doi.org/10.1002/pi.3144
16. Chen T, Liu H, Wang X, Zhang H, Zhang X (2018) Properties and fabrication of PA66/surface-modified multi-walled nanotubes composite fibers by ball milling and melt-spinning. Polymers 10:547–560. https://doi.org/10.3390/polym10050547
17. Socher R, Krause B, Boldt R, Hermasch S, Wursche R, Pötschke P (2011) Melt mixed nano composites of PA12 with MWNTs: influence of MWNT and matrix properties on macrodispersion and electrical properties. Compos Sci Technol 71:306–314. https://doi.org/10.1016/j.compscitech.2010.11.015
18. Meng H, Sui GX, Fang PF, Yang R (2008) Effects of acid- and diamine-modified MWNTs on the mechanical properties and crystallization behavior of polyamide 6. Polymer 49:610–620. https://doi.org/10.1016/j.polymer.2007.12.001
19. Jeon HS, Rameshwaram JK, Kim G, Weinkauf DH (2003) Characterization of polyisoprene–clay nanocomposites prepared by solution blending. Polymer 44:5749–5758. https://doi.org/10.1016/S0032-3861(03)00466-X
20. Zhou LF, Liu HH, Zhang XX (2015) Graphene and carbon nanotubes for the synergistic reinforcement of polyamide 6 fibers. J Mater Sci 50:2797–2805. https://doi.org/10.1007/s10853-015-8837-z
21. Zhao C, Hu G, Justice R, Schaefer DW, Zhang S, Yang M, Han CC (2005) Synthesis and characterization of multi-walled carbon nanotubes reinforced polyamide 6 via in situ polymerization. Polymer 46:5125–5132. https://doi.org/10.1016/j.polymer.2005.04.065
22. Mehdi SK, Vahid HA, Farid BS, Saeid RR, Hossein RM, Mahmoud H (2012) Effect of carbon nanotubes on the kinetics of in situ polymerization of methyl methacrylate. Nano Brief Reports and Reviews 7:1250003. https://doi.org/10.1142/S1793292012500038
23. Xie L, Li P, Ma Y, Sha J (2012) A representation method for describing a deagglomerating process in continuous mixer. Polym Compos 33:476–483. https://doi.org/10.1002/pc.22135
24. Liu RJ, Zhao FH, Zhang HH, Yu XY, Ding HL (2015) Preparation of polyimide/MWCNT nanocomposites via solid state shearing pulverization (S3P) processing. J Nanosci Nanotechnol 15:3780–3785. https://doi.org/10.1166/jnn.2015.9490
25. Javed H, Islam M, Mahmood N, Achour A, Hameed A, Khatri N (2016) Catalytic growth of multi-walled carbon nanotubes using NiFe2O4 nanoparticles and incorporation into epoxy matrix for enhanced mechanical properties. J Polym Eng 36:53–64. https://doi.org/10.1515/polyeng-2015-0137
26. Allen MJ, Tung VC, Kaner RB (2009) Honeycomb carbon: a review of graphene. Chem Rev 110:132–145. https://doi.org/10.1021/cr900070d
27. Scaffaro R, Maio A, Tito AC (2012) High performance PA6/CNTs nanohybrid fibers prepared in the melt. Compos Sci Technol 72:1918–1923. https://doi.org/10.1016/j.compscitech.2012.08.010
28. John HL, Mauricio T, Elisabeth M, Katherine EH, Vincent M (2011) Evaluating the characteristics of multiwall carbon nanotubes. Carbon 49:2581–2602. https://doi.org/10.1016/j.carbon.2011.03.028
29. Hwang YG, Lee SC, Jeong YG (2014) Structure, electrical and mechanical properties of polyamide 66/acid-treated MWCNT composite films prepared by solution mixing in the presence of nonionic surfactant. Fibers Polym 15:1010–1016. https://doi.org/10.1007/s12221-014-1010-5
30. Zabihi O, Ahmadi M, Abdollahi T, Nikafshar S, Naebe M (2017) Collision-induced activation: towards industrially scalable approach to graphite nanoplatelets functionalization for superior polymer nanocomposites. Sci Rep 7:3560. https://doi.org/10.1038/s41598-017-03890-8
31. Yang Y, Zhao M, Xia Z, Duan H, Zhao G, Liu Y (2018) Facile preparation of polyamide 6/exfoliated graphite nanoplate composites via ultrasound-assisted processing. Polym Eng Sci 58:1739–1745. https://doi.org/10.1002/pen.24773
32. Zhou JL, Wang QQ, Jia C, Innocent MT, Pan WN, Xiang HX, Zhu MF (2021) Molecular weight discrete distribution-induced orientation of high-strength copolyamide fibers: effects of component proportion and molecular weight. Macromol 54:7529–7539. https://doi.org/10.1021/acs.macromol.1c00915
33. Pan W, Zhou J, Xiang H, Innocent MT, Zhai G, Zhu M (2020) Melt-spun industrial super-strong polycaprolactam fiber: effects of tie-molecules and crystal transformation. COMPOS PART

B-ENG 185:107772. https://doi.org/10.1016/j.compositesb.2020.107772

34. Armas J, Reynolds K, Marsh Z, Fernández-Blázquez J, Ayala D, Cronin A, Aguila J, Fideldy R, Abdou J, Bilger D, Vilatela J, Stefik M, Scott G, Zhang S (2019) Supramolecular assembly of oriented spherulitic crystals of conjugated polymers surrounding carbon nanotube fibers. Macromol Rapid Commun 40:1900098. https://doi.org/10.1002/marc.201900098
35. Scaffaro R, Maio A (2017) A green method to prepare nanosilica modified graphene oxide to inhibit nanoparticles re-aggregation during melt processing. Chem Eng J 308:1034–1047. https://doi.org/10.1016/j.cej.2016.09.131